Influence of Refractive Index Distribution on Brillouin Gain Spectrum in GeO_2-Doped Optical Fibers

JI Zhengyuan[1,2], *LU Yuangang*[1,2*], *PAN Yuhang*[2,3], *PENG Jianqin*[1,2], *ZHANG Zelin*[1,2], *WANG Jiming*[2]

1. Key Laboratory of Space Photoelectric Detection and Perception of Ministry of Industry and Information Technology, College of Astronautics, Nanjing University of Aeronautics and Astronautics, Nanjing 211106, P. R, China;
2. College of Science, Nanjing University of Aeronautics and Astronautics, Nanjing 211106, P. R. China;
3. Shanghai Aircraft Design and Research Institute, Shanghai 200120, P. R. China

(Received 10 March 2020; revised 12 March 2021; accepted 20 May 2021)

Abstract: GeO_2 is commonly used as dopant to adjust the refractive index profile (RIP) and the acoustic velocity profile (AVP) in the fiber, thereby forming different Brillouin gain spectrum (BGS) characteristics such as Brillouin gain, acoustic mode number and peak intensity difference. When an optical fiber is used in optical fiber sensing or communication system, its BGS characteristics may play an important role in determining the performance of the system. In this paper, finite element analysis (FEA) method is used to study the influence of refractive index distribution and its corresponding AVP on the BGS in step-index, graded-index, and complex-index optical fibers. A new method has also been proposed to efficiently discriminate acoustic mode solution and obtain the new and full images of total Brillouin gain and acoustic modes number of the fiber as a function of the refractive index distribution, considering the influence of changing the refractive index difference and the geometric size simultaneously. For each type of optical fiber, the recommended parameter range is provided for optical fiber sensing and optical fiber communication. Moreover, the suitable optical fiber with close peak intensity in its multi-peak BGS is explored and achieved, which can be used in Brillouin beat spectrum detection systems to improve sensing accuracy.

Key words: Brillouin gain spectrum; optical fiber; acoustic mode; refractive index; finite element analysis(FEA)

CLC number: O437.2 **Document code:** A **Article ID:** 1005-1120(2021)05-0769-19

0 Introduction

Stimulated Brillouin scattering (SBS) is a nonlinear phenomenon caused by the interaction between optical and acoustic waves[1-3]. Several acoustic modes can be excited in a single-mode fiber (SMF) which has a complex refractive index distribution. This determines the corresponding Brillouin gain spectrum (BGS) has multi-Brillouin peaks[4-5]. These properties effectively decrease the Brillouin gain in unit area within the core of the fiber, therefore, improving the SBS threshold which allows higher input optical power in the fiber to reach longer transmission distance and higher signal to noise ratio (SNR).

Many studies have been carried out to research the characteristics of different acoustic modes or the interaction between acoustic modes and optical fundamental mode in different kinds of fibers[5-10]. Some of these characteristics have been applied beneficially in distributed fiber sensing systems[4-5, 11-16]. For example, the large effective area fiber (LEAF, made by Corning Inc.) is a kind of non-zero dispersion-shifted fiber (NZDSF) with several acoustic modes, which can be utilized as the sensing fiber in Brillouin optical time domain analysis (BOTDA) system[4] and Brillouin optical time domain reflec-

*Corresponding author, E-mail address: luyg@nuaa.edu.cn.

How to cite this article: JI Zhengyuan, LU Yuangang, PAN Yuhang, et al. Influence of refractive index distribution on Brillouin gain spectrum in GeO_2-Doped optical fibers[J]. Transactions of Nanjing University of Aeronautics and Astronautics, 2021, 38(5): 769-787.

http://dx.doi.org/10.16356/j.1005-1120.2021.05.006

tometry (BOTDR) system[12]. In our previous study[12], the homodyne BOTDR system is based on measuring the peak power of Brillouin beat spectrum (BBS) in LEAF. Actually, due to their diverse refractive index distribution, different kinds of fibers have distinct BGS characteristics such as Brillouin gain, acoustic mode number and peak intensity difference. That may affect the measurement accuracy and efficiency of the optical fiber sensing system, and the transmission performance of optical fiber communication systems.

With the advancement of fiber-optic communication and Brillouin sensing technology, it is necessary to know the comprehensive relationship between the refractive index distribution and the BGS. In the previous studies, the effect of dopant concentration on the BGS was studied. These dopants include commonly used GeO_2 and F[7,17-19], as well as some special materials such as As_2Se_3, tellurite, and bismuth[3, 20-22]. The BGSs of fibers have been explored by changing the geometry or refractive index difference[23-24]. However, there is no related research performed from the perspective of changing the fiber refractive index difference and geometric size simultaneously. To our knowledge, the effects of numerous possibilities for refractive index distribution on the shape of BGS have not been considered nor investigated. Until now, a full image of the effect of the refractive index profile on the BGS is still missing, although various commercial GeO_2-doped fibers have been used in a large number of applications.

To this end, all the possibilities of the refractive index distribution of the GeO_2-doped optical fibers are considered, including the influence of changing the refractive index difference and the geometric size simultaneously. We present the new and full images of Brillouin gain and acoustic modes number of the fiber as a function of the refractive index distribution. The influence of refractive index distribution on the BGS characteristics in common GeO_2-doped fibers (including step-index, graded-index and complex-index optical fibers) are analyzed by using finite element analysis (FEA) method.

When using FEA software to solve the acoustic field distribution in the fiber, it is usually necessary to set a larger desired number of eigenvalues than the actual acoustic mode number. For example, when simulating an acoustic multimode fiber, it is usually need to set the desired number of eigenvalues to dozens to find two or three circularly symmetric solutions. When simulating a fiber with a specific structure, we can artificially observe these dozens of solutions and eliminate the pseudo-solutions to obtain circularly symmetric acoustic modes. However, if a study of a large quantity of fiber structure parameter combinations is required, artificially identifying the solutions is a very inefficient strategy. In order to solve this problem, an innovative method will be proposed that can be used to quickly determine the circular symmetry of the acoustic field.

For the three kinds of common fibers, the relationship between refractive index distribution and BGS characteristics (total Brillouin gain, acoustic mode number, and peak intensity difference) will be discussed. Furthermore, in order to realize more effective homodyne BOTDR system based on BBS detection[12], the suitable fiber structural parameters to achieve multi-peak BGS with close peak intensity are also studied. The new results obtained in this paper may benefit in designing new optical fiber and choosing the optimal optical fiber to be used in sensing and communication systems. Besides, the analysis described in this paper may be of significant value in the search for high Brillouin gain fibers with multi-peak Brillouin spectrum, and provides a guide for designing suitable solid optical fibers applied in the Brillouin scattering based fiber sensing systems.

1 Principles

1.1 Brillouin gain spectrum

According to previous studies[10,25-26], the occurrence of Brillouin scattering comes along with the propagation of acoustic modes during the SBS process. The SBS process is governed by the following set of two coupled equations[1, 26]

$$\frac{\mathrm{d}I_\mathrm{P}}{\mathrm{d}z} = -g_\mathrm{m}(\nu) I_\mathrm{P} I_\mathrm{S} - \alpha I_\mathrm{P} \tag{1}$$

$$\frac{\mathrm{d}I_S}{\mathrm{d}z} = -g_m(\nu)I_P I_S - \alpha I_S \tag{2}$$

where I_S and I_P are the Stokes and pump waves, respectively, and α is the linear loss coefficient of optical waves. When more than one Brillouin scattering active acoustic modes exist in fibers, each acoustic mode is responsible for a spectral feature in the BGS. The Brillouin gain spectrum corresponding to the mth acoustic mode can be expressed as

$$g_m(\nu) = g_m \cdot \frac{(\omega_m/2)^2}{(\nu - \nu_p + \nu_m/2)^2 + (\omega_m/2)^2} \tag{3}$$

where ν is the frequency of scattered light, ν_p is the incident light frequency, and ν_m and ω_m are the frequency shift and the full width at half maximum (FWHM) of the mth peak in the BGS, respectively. The peak Brillouin gain of the mth acoustic mode is

$$g_m = \frac{4\pi p_{12}^2 n_{\mathrm{eff}}^8 f_m^A}{c\lambda^3 \rho_0 \omega_m \nu_m} \tag{4}$$

where p_{12} is the respective component of the electrostriction tensor, c the velocity of light, λ the optical wavelength of the incident light in vacuum, n_{eff} the effective refractive index of the fundamental optical mode, ρ_0 the mean value of the material density of the fiber, and f_m^A the fraction by which the SBS gain is reduced if the mth acoustic and optical modes do not fully overlap inside the fiber[27-28].

$$f_m^A = \frac{A_{\mathrm{eff}}}{A_m^{ao}} \tag{5}$$

where A_{eff} and A_m^{ao} are named optical effective area and acousto-optic effective area, shown as

$$A_{\mathrm{eff}} = \frac{\left[\iint E^2(x,y)\mathrm{d}x\mathrm{d}y\right]^2}{\iint E^4(x,y)\mathrm{d}x\mathrm{d}y} \tag{6}$$

$$A_m^{ao} = \left[\frac{\iint E^2(x,y)\mathrm{d}x\mathrm{d}y}{\iint E^2(x,y)u_m(x,y)\mathrm{d}x\mathrm{d}y}\right]^2 \iint u_m^2(x,y)\mathrm{d}x\mathrm{d}y \tag{7}$$

Indeed, dopant concentration in the fiber will affect p_{12}, ρ_0, and ω_m. However, the changes in these parameters are quite small and do not influence the shape of the BGS. For example, when the doping concentration of GeO_2 is from 2% to 10%, the corresponding ω_m is from 35 MHz to 45 MHz[18]. In this work 40 MHz is utilized as FWHM of each peak in BGS to calculate the peak Brillouin gain as the BGS linewidths obtained from the fiber structure parameters involved are around this value[29-30].

As shown in Eq.(3), each acoustic mode in a fiber corresponds to a Brillouin gain peak with the Lorentz shape. If there is more than one acoustic mode in a fiber, the shape of the BGS maybe has multi-peaks. The total BGS of the fiber is the sum of the BGSs of individual acoustic modes, and can be expressed as

$$G(v) = \sum_m g_m(\nu) \tag{8}$$

In Eq.(7), $E(x,y)$ and $u_m(x,y)$ are horizontal profiles of the fundamental optical and the mth acoustic mode of the fiber, respectively. They can be calculated from the following 2-D scalar optical propagation Eq.(9) and mechanical Eq.(10) equations by using FEA method[8].

$$\nabla_t^2 E(x,y) + \left(\frac{2\pi}{\lambda}\right)^2 (n^2 - n_{\mathrm{eff}}^2) E(x,y) = 0 \tag{9}$$

$$\nabla_t^2 u(x,y) + \left(\frac{\omega_{\mathrm{aco}}^2}{V_l^2} - \beta_{\mathrm{aco}}^2\right) u(x,y) = 0 \tag{10}$$

where ∇_t^2 is the transverse Laplacian operator in the (x, y) plane, n the refractive index of the fiber, and β_{aco} the propagation constant of the acoustic mode and given as $\beta_{\mathrm{aco}} = 4\pi n_{\mathrm{eff}}/\lambda$. ω_{aco} is the angular frequency of the acoustic wave, $\omega_{\mathrm{aco}} = 2\pi\nu_m$, which can be calculated by FEA method. V_l is the longitudinal sound velocity which can be obtained from the following empirical relation[2]

$$V_l = 5\,944\left[1 - 7.8\frac{n(r) - n_{SiO_2}}{n_{SiO_2}}\right] \tag{11}$$

where the 5 944 m/s is the longitudinal sound velocity in pure silica. When dopant is GeO_2, the refractive index of the core is increased and the sound velocity in the longitudinal direction is lowered. The refractive indices of the fibers referred to herein are all adjusted by doping GeO_2. So, the refractive index distribution we consider is actually determined by the material and geometry of the fiber[3,7].

According to Eq.(3) to Eq.(11), when the refractive index distribution of a fiber is known, we can obtain the optical mode and acoustic modes dis-

tribution, as well as the number of acoustic modes and the BGS of the fiber. Therefore, the fiber parameters such as core radius and refractive index difference can be adjusted, and thus we can obtain a comprehensive view of the relationship between the number of acoustic modes and the Brillouin gain as a function of refractive index distribution.

The shape of BGS of some kind fibers has multi-peaks, and thus the commonly used peak Brillouin gain, g_m, in Eq.(4) cannot effectively reflect the level of total Brillouin gain of fibers, as mentioned above. In this paper, a new parameter is defined, the total Brillouin gain, g_{B_total}, to evaluate the total Brillouin gain of different GeO_2-doped fibers. After obtaining the BGS of a fiber, $G(\nu)$, the total Brillouin gain of the fiber can be obtained by calculating the integral of BGS on the frequency domain. It can be expressed as

$$g_{B\_total} = \int G(\nu)\mathrm{d}\nu \tag{12}$$

It should be noted that both of the values and units of g_{B_total} and g_m are different. For example, when the optical wavelength of the incident light is 1 550 nm, the peak Brillouin gain of SMF-28 fiber, g_m, obtained with Eq.(4) is 1.63×10^{-11} m/W, while its corresponding total Brillouin gain, g_{B_total}, is 1×10^{-3} m/(W·s) which is obtained by Eq.(12).

1.2 Acoustic mode solution discriminating

In the process of solving the acoustic mode solution by FEA, in order to effectively discriminate the actual acoustic mode solution from dozens of eigenvalues, a novel acoustic mode solution discriminating method is proposed.

In general, the cross section of the fiber is defined as the x-y coordinate plane and the fiber axis is defined as the coordinate origin in FEA calculation. The obtained acoustic field $u(x, y)$ is output in the form of a grid. Then we convert $u(x, y)$ from a Cartesian coordinate system to a polar coordinate system $u(r, \theta)$ by $r=\sqrt{x^2+y^2}$ and $\theta=\arctan(y/x)$. And we divide the polar coordinate plane from the origin into N equal sectors. In a circularly symmetric acoustic mode, the sum of $u(r, \theta)$ in each sector should be equal. In other words, the sum of $u(r, \theta)$ in the ith and jth regions ($1 \leqslant i < j \leqslant N$) should be nearly equal, which is

$$\frac{\left|\sum_{2\pi(i-1)/N\leqslant\theta\leqslant 2\pi i/N} u(r,\theta) - \sum_{2\pi(j-1)/N\leqslant\theta\leqslant 2\pi j/N} u(r,\theta)\right|}{\left|u_{\max}(r,\theta)\right|} < \delta_1 \tag{13}$$

where $u_{\max}(r,\theta)$ is the maximum of all acoustic mode solutions and δ_1 the small constant. We can take the value of δ_1 as $10^{-5}\ u_{\max}(r,\theta)$ in the calculation process.

We can exclude some pseudo solutions of $u(r,\theta)$ by the above method. In the remaining solutions, we estimate the degree of numerical dispersion over each radius and obtain the solution of circular symmetric distribution. We select K radius (r_1, $r_2, \cdots, r_l, \cdots, r_K$, $1 \leqslant l \leqslant K$) by a certain step size on the plane of the acoustic mode solution to calculate the standard deviation of $u(r_l, \theta)$ on each radius of r_l. In a circularly symmetric acoustic mode solution, these standard deviations should satisfy

$$\frac{\sqrt{\frac{1}{M}\sum_{\theta=0}^{2\pi}\left[u(r_l,\theta)-\overline{u(r_l,\theta)}\right]^2}}{\left|\overline{u(r_l,\theta)}\right|} \leqslant \delta_2 \tag{14}$$

where M is the total number of acoustic field data points on the radius r_l, $\left|\overline{u(r_l,\theta)}\right|$ the average of $u(r_l,\theta)$ on the radius r_l, δ_2 the small constant and we take the value of δ_2 as 10^{-4} in the calculation process. If both Eqs. (13,14) are satisfied, it can be inferred that the acoustic field is circularly symmetric.

2 Influence of Refractive Index Distribution on BGS

According to refractive index distribution, solid optical fibers generally can be divided into three categories including step-index optical fiber (SIOF), graded-index optical fiber (GIOF), and complex-index optical fiber (CIOF). The effects of dopant concentration of GeO_2 on the BGS in single-mode fibers have been studied[7,17-19]. However, these studies only discuss the cases where only one parameter changes and one parameter cannot describe the overall refractive index distribution. In

this section, the effects of refractive index difference and geometry on the shape of the BGS are studied. We will consider the myriad possibilities of combining these two variables, and obtain the full image of the effect of the refractive index profile on the BGS. We will present the relationship between refractive index distribution and BGS characteristics (Brillouin gain, acoustic mode number, and peak intensity difference), and we also discuss whether there are suitable fiber structural parameters to achieve multi-peak BGS with close peak intensity in each fiber category.

2.1 Verification of simulation method

To illustrate the accuracy of our simulation method based on FEA method, we have simulated a graded-index fiber doped with GeO_2 in Ref.[10]. This paper gives the refractive index profile and the measurement results of the BGS of the fiber. Fig.1 shows the actual refractive index profile of the fiber. The measured BGS of the fiber and our simulation results are shown in Fig.2.

From Fig.2, we can see that the BGS of the fiber obtained by the FEA method is very consistent with the experimental measurement results. The frequency shift and relative power comparison of Peak 1—3 of BGSs in Fig.2 is given in Table 1. The relative error of the Brillouin frequency shift between simulation and experiment is within 0.5%, which indicate that our results are in good agreement with the experiment. The simulation errors relative to the measured relative power of the three peaks are 0%, 7.1% and 8.8%, respectively. Therefore, the difference between the simulation and the experimental BGSs is very small. These errors may be caused by imperfections in the production process during fiber drawing.

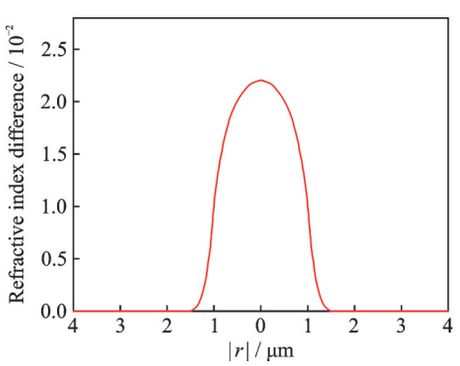

Fig.1 RIP of fiber in Ref.[10]

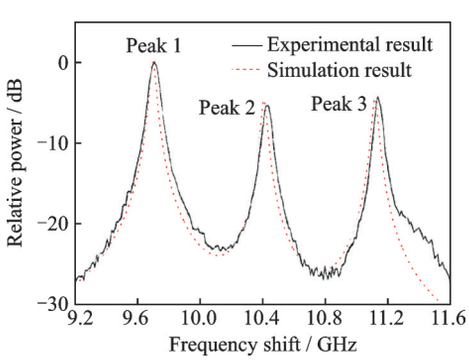

Fig.2 Simulated and measured BGSs of fiber

Table 1 Comparison of simulated and measured BGSs

Parameter	Brillouin frequency shift/GHz			Relative power/dB		
	Peak 1	Peak 2	Peak 3	Peak 1	Peak 2	Peak 3
Our results	9.70	10.41	11.12	0	−4.9	−4.8
Ref.[10]	9.72	10.44	11.17	0	−5.2	−4.4
Relative error/%	0.21	0.19	0.36	0	7.1	8.8

2.2 Step-index optical fiber (SIOF)

The standard single mode fiber (SMF-28) can be considered as a representative of SIOFs. The RIP and AVP of SMF-28 are shown in Fig.3. The parameters of SMF-28 at wavelength 1 550 nm can be obtained by referring to previous paper[31]. n_1 and n_2 in Fig.3 are the core and cladding refractive indices, respectively. a is the core radius. The AVP is determined by the RIP according to Eq.(11). In the following, when talking about the change of the refractive index, the acoustic velocity of the fiber is regulated accordingly.

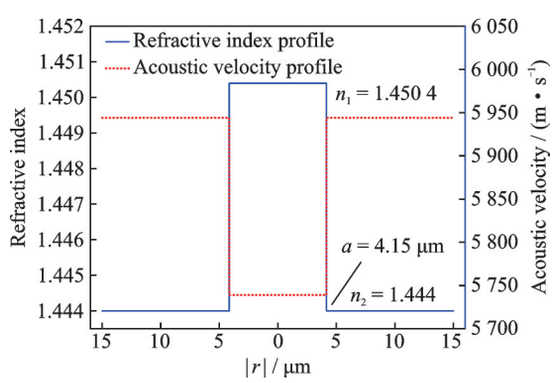

Fig.3 RIP and AVP of SMF-28 at wavelength 1 550 nm

In the case of general SIOFs, the refractive index distribution of the optical fiber depends on two factors, the core radius and the refractive index difference. In order to describe the changes in BGS with refractive index distribution, we firstly determine the suitable range of core radius a and the refractive index difference Δ, which can be expressed as

$$\Delta = \frac{n_1^2 - n_2^2}{2n_1^2} \approx \frac{n_1 - n_2}{n_1} \tag{15}$$

When considering the core radius of the fiber, taking into account the limitations of the manufacturing process and taking the SMF-28 as a reference, we set the core radius a from 1 μm to 4.5 μm. As for the range of n_1, since n_1 must be greater than n_2 in a solid fiber, we set the minimum of n_1 as 1.446 which is slightly larger than n_2, as shown in Fig.3. To ensure that the fiber is a single mode fiber, when changing the core radius, the maximum value of n_1 is limited based on the single mode cut-off condition V_c=2.405 (V_c is optical fiber normalized frequency) at the corresponding radius. Furthermore, the refractive index difference Δ can be determined by using the relationship between the refractive index difference and the fiber loss due to the Rayleigh scattering. The acceptable fiber loss is less than 0.5 dB/km. The fiber loss in a single-mode fiber doped with GeO_2, α_{SR}, can be expressed as[32]

$$\alpha_{SR} = \frac{0.63}{\lambda^4}(1 + 180 \times \Delta)\ (\mathrm{dB/km}) \tag{16}$$

According to Eq.(16), when the radius is less than 2 μm, the core refractive index n_1 can reach a maximum of 1.474 2. When the core radius a increases from 2 μm, the maximum value of n_1 decreases according to the single mode cut-off condition. Thus, the upper-right boundary of parameter space (a, n_1) can be determined and it looks like an exponential decay curve. Therefore, the range of core radius and the core refractive index can be determined, as shown in Fig.4. By using the FEA method, the total Brillouin gain g_{B_total} and acoustic mode number can be obtained from Eq.(12) and Eq.(10), respectively. The profiles of total Brillouin gain g_{B_total} and acoustic mode number are shown in Fig.4(a) and Fig.4(b), respectively. We can obtain other parameters of BGS, such as Brillouin frequency shift and peak relative intensity. Since these results cannot be clearly presented in a 2-D graph, only the total Brillouin gain and the number of acoustic modes are displayed here.

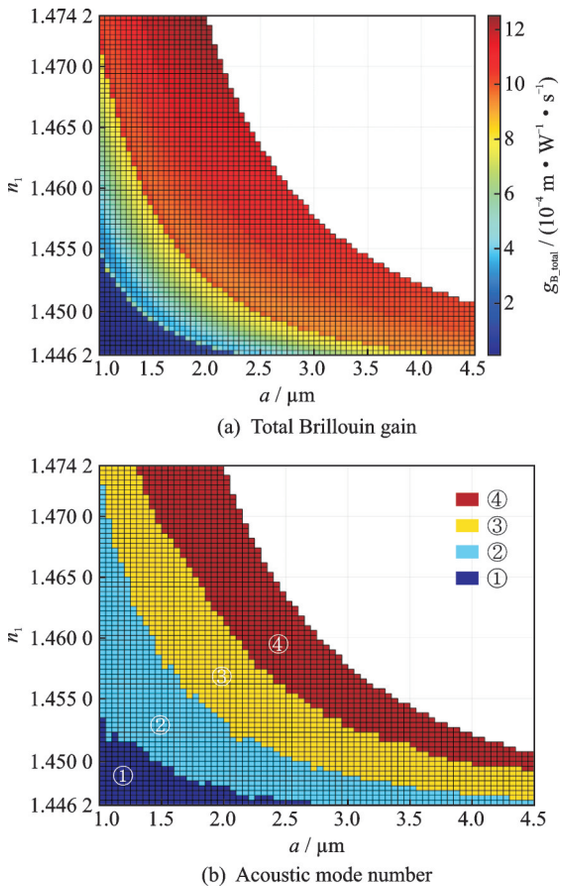

Fig.4 Simulation results of SIOFs

From Fig.4(a), we can see that in the upper right region of (a, n_1) combination, SIOFs have high Brillouin gain. Specially, the highest Brillouin gain area corresponds to the region where the core radius is from 1.4 μm to 2 μm and the core refractive index is from 1.467 to 1.474 2. In addition, as the core radius and refractive index increase, the number of acoustic modes guided in the fiber gradually increases. The distribution of the number of acoustic modes is basically consistent with the Brillouin gain distribution shown in Fig.4(a). The numbers marked in each area in Fig.4(b) denote the numbers of acoustic modes guided in the fiber. It should be noted that, according to the single mode cut-off condition, the sector in the upper right cor-

ner is out of consideration. The lower left corner of Fig.4 shows the fiber with a small refractive index difference and a small diameter. From the simulation results, these fibers have only one acoustic mode, and the total Brillouin gain is also the smallest. In fact, the bending losses of these fibers are very large, so they have no practical value. In order to clearly show the relationship between the shape of BGS and the fiber parameters, we select one point in each region randomly as a representative example and present the BGS of these particular fibers except for the 4th spectrum, as shown in Fig. 5. Since the total Brillouin gain g_{B_total} of the 4th spectrum is the largest in this paper, the first peak of the 4th spectrum is set as 0 dB, and all other BGSs in Fig.4 and below are plotted with respect to this value.

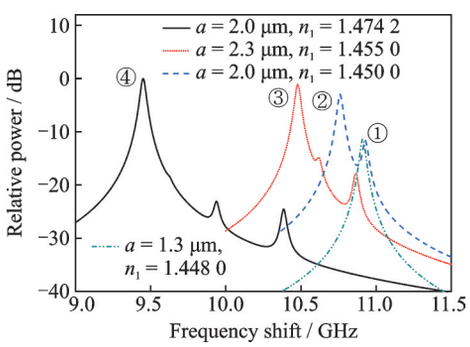

Fig.5 BGSs of SIOFs in four different areas

As can be seen from Fig. 5, the 4th spectrum represents the BGS from the area ④ in Fig.4(b). This BGS has the largest Brillouin peak gain. Since the frequency shift difference between the first acoustic mode and the second acoustic mode is small, the Brillouin peak contributed by the second acoustic mode (The corresponding frequency shift is 9.63 GHz) is enveloped by the first main peak of the BGS, and it only shows a minor protrusion. In this BGS, the third and fourth peaks are approximately 24 dB weaker than the first peak. For the 2nd and the 3rd spectra, we find that their total power gradually decreases compared to the 4th spectrum. As for the 1st spectrum, there is only one peak and the peak power is also the smallest. These results in Brillouin gain are consistent with that shown in Fig.4(a). Specifically, the two peaks in the 2nd spectrum are closer in intensity, since its second peak is only 8.6 dB weaker than the first peak. The 3rd spectrum has three peaks, and its second and third peaks are 13.7 and 16.7 dB weaker than the first peak, respectively.

Generally, SBS is a harmful nonlinear optical phenomenon in the field of optical fiber communication, which attenuates the power of the signal, thereby reducing the communication distance and the system SNR[33-34]. For the application of step-index fiber in optical fiber communication, fibers with lower total Brillouin gain g_{B_total} perform better, as shown in the region from the yellow to light blue color in Fig.4(a). This region corresponds to most of the area where the number of acoustic mode is 2, as shown in Fig.4(b). Meanwhile, the fibers with high Brillouin gain, as shown in the upper right region in Fig.4(a), can be used as ideal sensing fibers.

2.3 Graded-index optical fiber (GIOF)

In GIOF, the refractive index of the core is variable. The refractive index decreases gradually from its maximum value n_1 at the core center to its minimum value n_2 at the core-cladding interface. The cladding usually has constant refractive index. Most GIOFs follow the g-type refractive index distribution which can be described as

$$n(r)=\begin{cases} n_1\left[1-2\Delta\left(\dfrac{r}{a}\right)^g\right]^{1/2} & 0\leqslant r\leqslant a \\ n_2 & r>a \end{cases} \tag{17}$$

where a is the core radius, and Δ the refractive index difference between the axis and the cladding. g determines the shape of the refractive index profile. When $g\to\infty$, the fiber is a step-index optical fiber. When $g=1$, 2, the fiber types are triangular-index fiber and parabolic-index fiber, respectively. In this paper the parabolic index fibers are used as research object since the refractive index profile of most graded-index fibers is parabolic. RIP and AVP of parabolic index fiber are shown in Fig.6.

As that shown in Fig.7, the ranges of n_1 and a of GIOFs can be determined similarly as that discussed in SIOFs. The upper-right boundary of parameter space (a, n_1) are calculated by considering

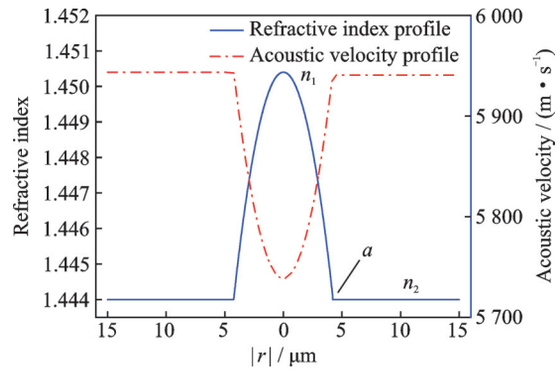

Fig.6 RIP and AVP of GIOF at wavelength 1 550 nm

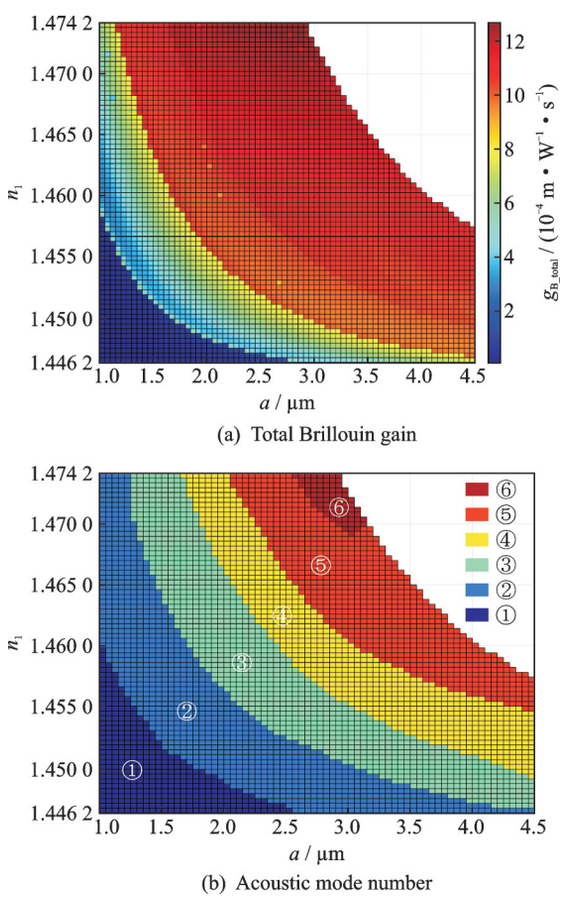

Fig.7 Simulation results of GIOFs

the single mode cut-off condition V_c=3.518 at the corresponding radius and the acceptable maximum fiber loss of 0.5 dB/km[35]. The profiles of total Brillouin gain g_{B_total} and acoustic mode number are calculated from Eq.(12) and Eq.(10) and shown in Fig.7(a) and Fig.7(b), respectively.

From Fig.7(a), we can observe that the Brillouin gain distribution of graded-index fiber is similar to that of SIOFs. The GIOFs with core radius ranging from 2.25 μm to 3 μm and axis refractive index from 1.468 to 1.474 2 has a higher Brillouin gain. The numbers marked in each area in Fig.7(b) represent the numbers of acoustic modes guided in the fiber. Unlike the case of SIOFs, the single-mode cut-off condition is V_c=3.518 in the parabolic-index fibers. The larger value of V_c results in the larger range of the refractive index distribution in GIOFs. Combining Fig.7(a) and Fig.7(b), the fiber that guides more acoustic modes usually has a higher Brillouin gain. This is similar to the case of step-index optical fibers. Similar to the SIOFs in Section 2.2, the fibers corresponding to the lower left corner region have no practical value.

Similarly, in order to clearly show the relationship between the shape of BGS and the fiber parameters, we select one point in each region in a random way as a representative example and describe the BGS of these particular fibers. The five different BGSs are shown in Fig.8.

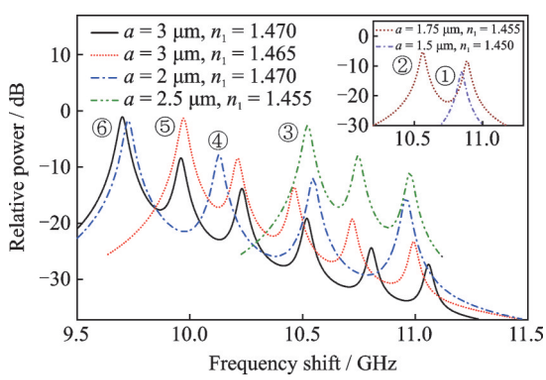

Fig.8 BGSs of GIOFs in six different areas

The 6th spectrum in Fig.8 is a typical BGS in the area ⑥ in Fig.7(b). This BGS has six peaks. As the frequency shift increases, the intensity of the peaks decreases 2.9—7.3 dB one by one, and the intensity difference between two adjacent peaks decreases. The 5th spectrum has five peaks, and its shape is similar to that of the 6th spectrum. The 4th and the 3rd spectrums represent BGS in area ④ and area ③ in Fig.7(b), respectively. For the 2nd and the 1st spectra, we find that their total Brillouin gains are less than that of the 6th and 5th spectra. As for the 1st spectrum, there is only one peak and the peak power is the smallest. These results related to Brillouin gain are consistent with that in Fig.7(a).

Similar to the case in Section 2.2, the optical fi-

bers with low total Brillouin gain g_{B_total} are suitable to be utilized in the fiber communication system. As shown in Fig.7(b), this kind of fiber has two acoustic modes guided in the fiber core. Fibers with high Brillouin gain are more suitable to the Brillouin sensing system, and their parameter pairs (a, n_1) are also in the upper right corner of Fig.7(a).

2.4 Complex index optical fiber (CIOF)

In order to achieve the lower loss, the lower dispersion, the lower bending sensitivity or the larger optical mode field area, some CIOFs have appeared. Common CIOFs include dispersion compensating fiber, depressed cladding fiber, bend insensitive fiber, double-clad fiber, and large effective area fiber. In this section, Corning large effective area fiber (LEAF) and trench assisted fiber (TAF) are chosen as the typical fibers.

2.4.1 Large effective area fiber (LEAF)

The actual refractive index profile of LEAF is shown in Fig.9(a)[2]. For the convenience of calculation, RIP and AVP of LEAF are simplified as shown in Fig.9(b). The simplified refractive index distribution of LEAF can be expressed as

$$n(r)=\begin{cases}n_1[1-2\Delta(r/a)]^{1/2} & 0\leqslant r<a\\ n_2 & b\leqslant r<c\\ n_3 & a\leqslant r<b, r\geqslant c\end{cases} \quad (18)$$

The difference between calculation results of the simplified and the actual situation is so small that can be neglected.

The triangle part is called inner core and has a radius of a. The high refractive index difference outer-ring section ranges from b to c. n_1, n_2, and n_3 are the refractive indices of the center, the outer-ring section, and the cladding, respectively. When a=3.8 μm, b=5 μm, c=10 μm, and n_1, n_2, and n_3 at wavelength 1 550 nm are 1.456 1, 1.446 4, and 1.444 (1.444 is the refractive index of fused silica at 1 550 nm[36]), respectively, we obtain the optical effective area A_{eff} and three acousto-optic effective areas A_1^{ao}, A_2^{ao}, and A_3^{ao}, as shown in Table 2. There are actually five peaks in our calculated BGS of LEAF, but the power of the 4th and 5th peaks is very low. Therefore, only the results of the first three peaks are given in Table 2 to compare with the results in Ref.[2]. We find that our results are consistent with that shown in Ref.[2].

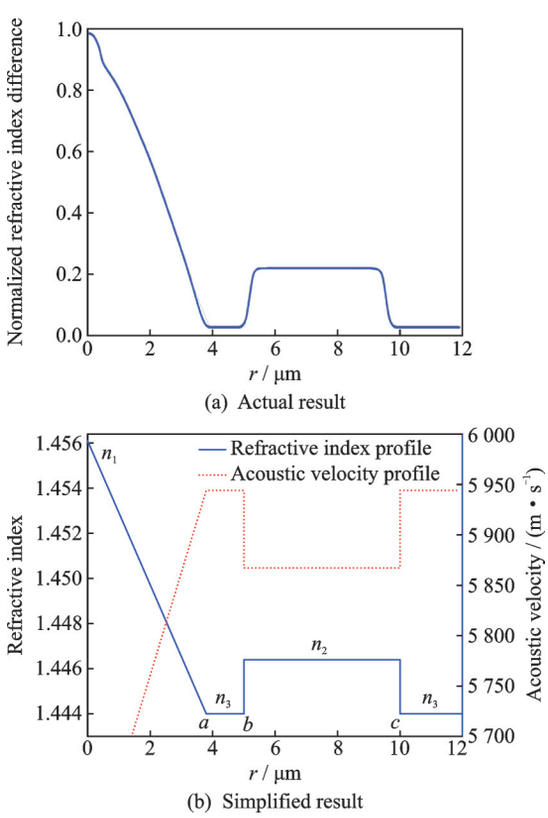

Fig.9 RIP and AVP of LEAF

Table 2 Parameter comparison of actual and simulated fibers

Parameter	A_{eff}/μm²	A_1^{ao}/μm²	A_2^{ao}/μm²	A_3^{ao}/μm²
Actual fiber	73.5	124.4	274.8	842
Our result	73.6	137.6	232.2	799

In LEAF with a complex refractive index distribution, there are many parameters that can be adjusted, including three radii a, b, and c and two refractive indices n_1 and n_2. In order to make the discussion more reasonable and simpler, we expect to find some important parameters that have a greater impact on BGS in these parameters. We firstly explore the effect of the outer-ring section on BGS by changing its width and distance from the center.

The position of the outer-ring section is changed. Here the width 5 μm remains unchanged. In other words, when b changes, c=(b+5) μm. When b changes from 4 μm to 12 μm, the corresponding BGSs are shown in Fig.10.

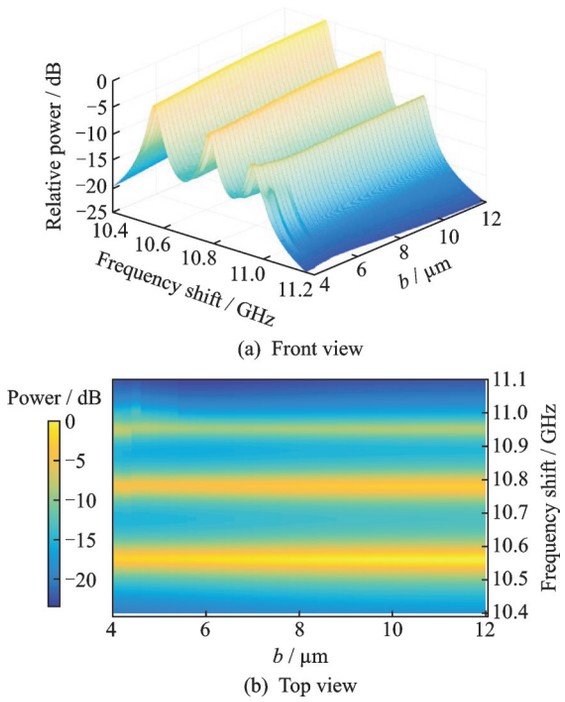

Fig.10 BGSs of LEAFs when b changing from 4 μm to 12 μm

Then we change the width of the outer-ring section. The value of c is changed while retaining the value of b as 5 μm. When c changes from 6 μm to 15 μm, the corresponding BGSs are similar to that shown in Fig. 10, so the figures are not presented here.

Therefore, only changing the position and width of the outer-ring section has little effect on the entire BGS. The geometric parameters of the outer ring affect the BGS weakly due to a very small part of the optical mode energy in this area.

Based on the above discussion, we could find three parameters that have a significant effect on BGS in LEAFs, namely the refractive indices n_1 and n_2, and the radius c. When c changes, a and b also change according to the original ratio. According to the Fig.9(b), we set $b=0.5c$ and $a=0.38c$. In such a case, the refractive index distribution of the fiber is determined by the three variables of n_1, n_2, and c. Here the total Brillouin gain g_{B_total} and the acoustic mode number actually are ternary functions. Therefore the result graph is a three-dimensional graph with the fourth dimension color-coded to indicate the magnitude of the value. The variation ranges of the three variables is shown in Table 3.

Table 3 Variation ranges of three variables

Variable	Variation range
n_1	1.445—1.475
n_2	1.444—1.464
c/μm	5—15

It can be seen from Table 3 that the range of n_1 indicates that the inner core index difference changes from 0.07% to the value that causes the largest fiber loss of 0.5 dB/km. The range of n_2 represents the outer-ring section grown out of nothing and its index difference increases from zero to 1.4%. The range of c means that all radius sizes can be adjusted to between 50% and 150% of the original size. The total Brillouin gain g_{B_total} changing with n_1, n_2, and c is shown in Fig.11. The acoustic mode number changing with n_1, n_2, and c is shown in Fig.12. The benefit of using a graph in the form of a cube is that it reflects the relationship of a function with three independent variables. These cube diagrams can fully demonstrate the effect of the refractive index distribution determined by the innumerable combination possibilities of these three variables on the total Bril-

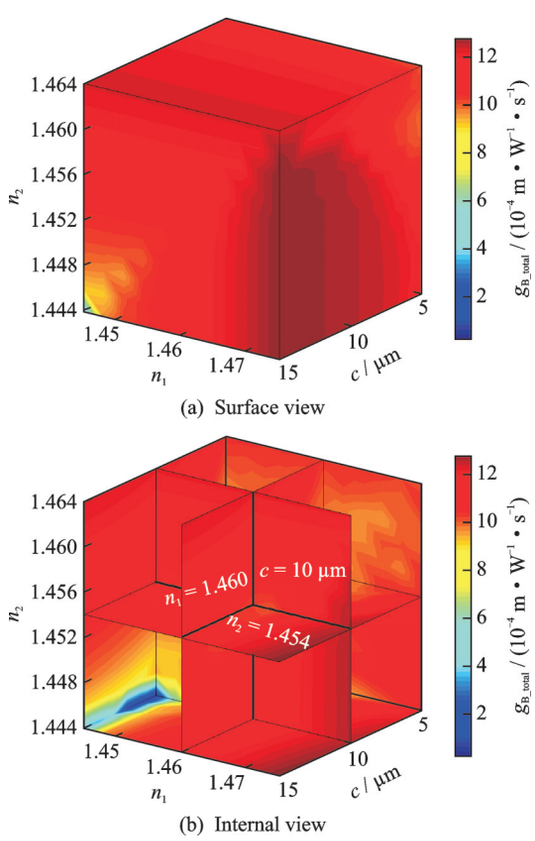

Fig.11 Total Brillouin gain g_{B_total} changing with n_1, n_2, and c

louin gain and the number of acoustic modes.

From surface of the cube shown in Fig.11(a), most areas have a high total Brillouin gain g_{B_total}. This is because LEAFs have a larger core radius than that of SIOFs and GIOFs, resulting in a larger optical effective area A_{eff}. In the range of c from 10 μm to 15 μm, n_1 from 1.472 to 1.475, and n_2 from 1.444 to 1.46, LEAFs have a higher total Brillouin gain. Fig. 11(b) is the internal view of the three-dimensional figure, where the three orthogonal planes are corresponded to c=10 μm, n_1=1.46, and n_2=1.454. We can see that the internal situation in total Brillouin gain is consistent with that on the surface, and the distribution of Brillouin gain is continuous without jumps or intervals. In the region of n_1=1.445 to 1.447 and n_2=1.444 to 1.446, LEAFs have a very low Brillouin gain. The refractive index difference between the core and the cladding and the refractive index difference between the outer ring and the cladding are very small, and their ability to restrain the optical field is weak, resulting in the optical field leakage. Fibers with this defect cannot be actually used. In general, with respect to the refractive index difference, the total Brillouin gain is positively correlated with n_1 and negatively correlated with n_2.

Fig. 12 illustrates that in the case of this complex structure, most fibers have more than five acoustic modes. Less acoustic modes are possible if the refractive index difference in the inner-core is very small. It can be concluded that the LEAFs have multiple acoustic modes. This also makes LEAFs exhibit a higher total Brillouin gain than that of SIOFs and GIOFs. Due to the complexity of structure, the distribution of the acoustic mode number does not appear to be regular. Similarly, to clearly show the relationship between the shape of BGS and the fiber parameters, we select several examples of different combinations of parameters and the BGSs of these representative fibers. The results are shown in Fig.13 and Fig.14. In order to ensure the clarity of the figure, only six spectra are painted in Fig.13. The BGSs of fibers with more acoustic modes are shown in Fig.14. These BGSs here are normalized to 0 dB according to the maximum gain of the 4th spectrum in Fig.5.

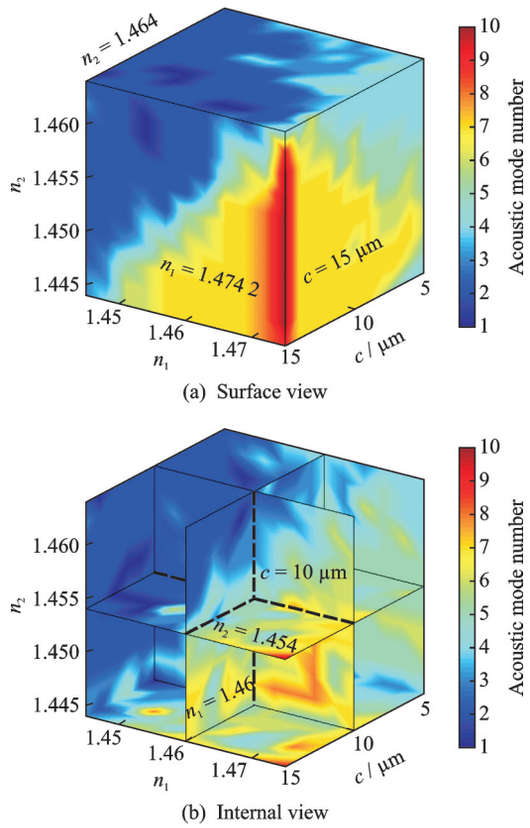

Fig.12 Acoustic mode number changing with n_1, n_2, and c

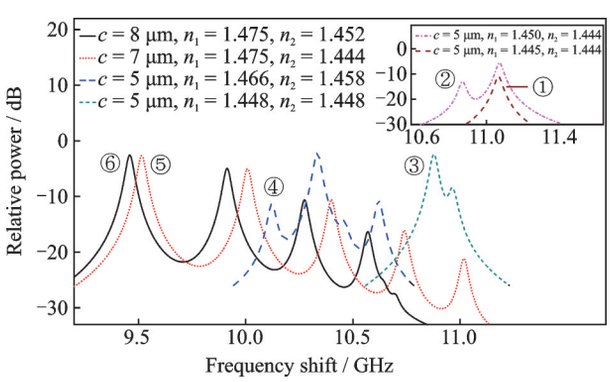

Fig.13 BGSs of six LEAFs with different n_1, n_2, and c

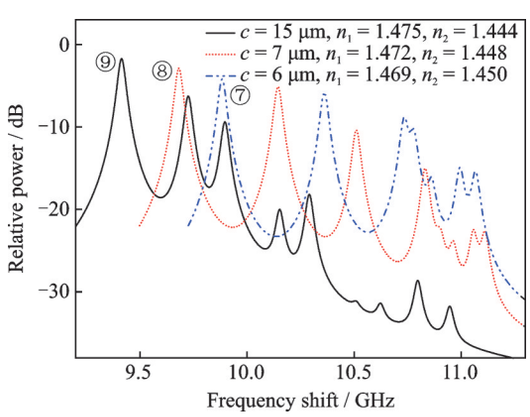

Fig.14 BGSs with more acoustic modes

In Fig.13, the numbers marked on these spectra represent the acoustic mode number of these fibers. For example, the 6th spectrum corresponds to the fiber with six acoustic modes. The fifth peak is located in 10.64 GHz and it is almost submerged by the fourth peak. The shape of the 5th spectrum looks very similar to that of the 6th spectrum. The relative power of their first three peaks is pretty close. For the 4th, 3rd, 2nd and 1st spectra, their total power gradually decreases compared with the 5th and 6th spectra. As for the 1st spectrum, there is only one peak and the peak power is also the smallest.

In Fig.12, some LEAF-type fibers have more than six or even ten acoustic modes. However, the intensities of the latter peaks in these BGSs are very weak relative to the main peak. We select some examples to illustrate this point. The detailed results are shown in Fig.14. Although there are nine acoustic modes in the 9th spectrum, the 4th and 5th peaks are weaker by about 18 dB with respect to the first peak, and the 6th and subsequent peaks are weaker by about 30 dB. These weak peaks can be ignored in practical applications.

Since the LEAFs have a large core radius and usually support five or more acoustic modes guided in the fibers, these reasons lead to higher total Brillouin gain, even if their peak gain are lower than that of the SIOFs. In LEAFs with c from 10 to 15, n_1 from 1.472 to 1.475, and n_2 from 1.444 to 1.46, they have higher total Brillouin gain and are more suitable for optical fiber Brillouin sensing. The multi-peak BGS caused by the multi-acoustic mode number makes LEAFs a better candidate for multi-parameter sensing. Optical fibers with the other parameter combinations in the cube shown in Fig.11 (a) are better used in optical fiber communication.

2.4.2 Trench assisted fiber (TAF)

The requirement of bend-insensitive optical fibers has led to the emergence of the trench assisted fiber. Refractive index trench is introduced into the cladding section in the TAF. Different from the above-mentioned types of optical fibers, fluorine is usually added to the silica fiber to achieve the low refractive index of the trench. Its typical RIP and AVP are shown in Fig.15.

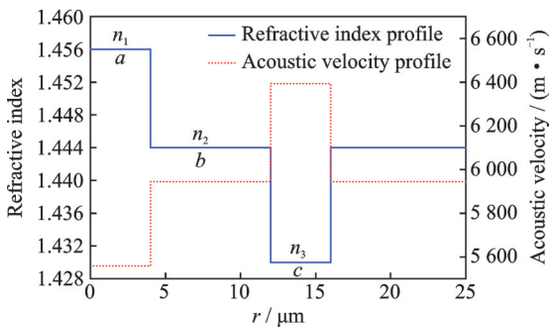

Fig.15 RIP and AVP of TAF

n_1, n_2 and n_3 in Fig.15 represent the refractive index of the core, inner/outer cladding and trench, respectively. And a, b and c in Fig.15 denote the core radius, inner cladding width and trench width, respectively. Therefore, the refractive index profile of the TAF can be expressed as

$$n(r)=\begin{cases} n_1 & 0\leqslant r<a \\ n_2 & a\leqslant r<a+b, r\geqslant a+b+c \\ n_3 & a+b\leqslant r<a+b+c \end{cases} \quad (19)$$

Three parameters, b, c and n_3, will change the refractive index distribution of trench, and thus affect BGSs of TAF. The same analysis method is adopted as that used in Section 2.4.1, changing the above three parameters separately to observe how TAF's BGS will change. The related parameters and variation ranges of the three parameters are shown in Table 4.

First, we change the depth of the trench, which is its refractive index n_3. b and c are set to be

Table 4 Parameters and variables of TAFs

Parameter	Value/Variation range
n_1	1.456
n_2	1.444
n_3	1.424—1.444
A / μm	4
b / μm	1—6
c / μm	1—11

3.5 μm and 6 μm, respectively. When n_3 changes from 1.424 to 1.444, the corresponding BGSs are shown in Fig.16.

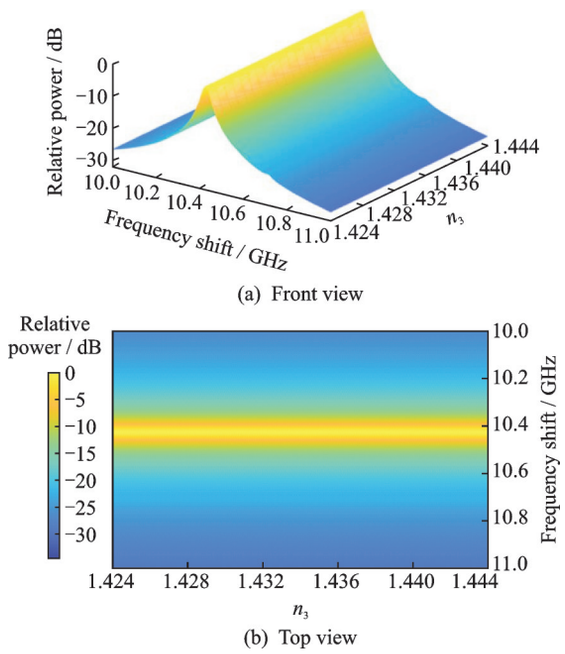

Fig.16 BGSs of TAFs when n_3 changing from 1.424 to 1.444

Next the width of the inner cladding section is changed. Here we keep c and n_3 fixed at c =6 μm and n_3=1.434 respectively and change the value of b. When b changes from 1 μm to 6 μm, the corresponding BGSs are shown in Fig.17.

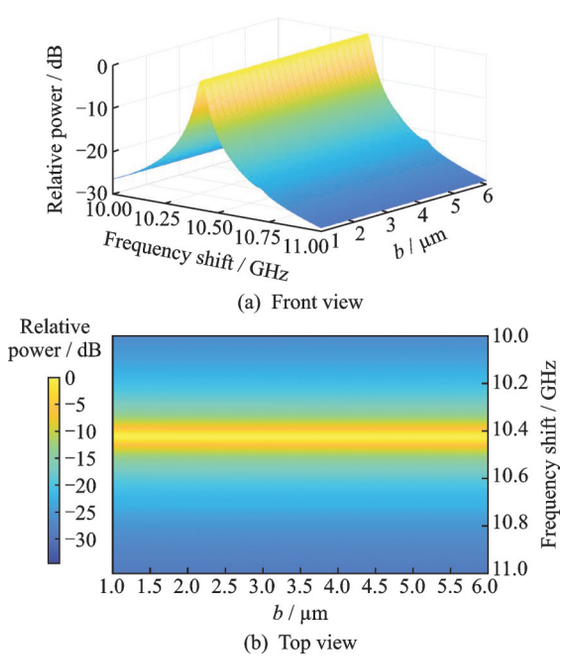

Fig.17 BGSs of TAFs when b changing from 1 μm to 6 μm

Finally, we set b and n_3 to be 3.5 μm and 1.434 respectively and change the c from 1 μm to 11 μm. BGSs of TAFs are shown in Fig.18.

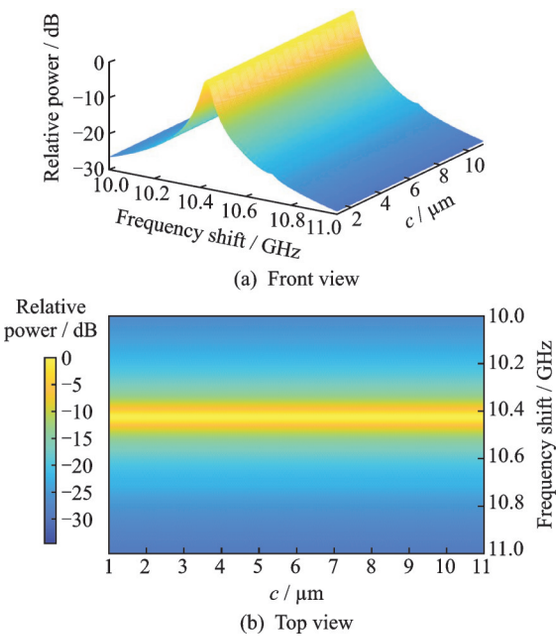

Fig.18 BGSs of TAFs when c changing from 1 μm to 11 μm

From the results shown in Fig. 16 to Fig. 18, changing the width of the inner cladding b, the width of the trench c and the refractive index of the trench n_3 does not make the BGS of the TAFs vary. The reason is that in the TAFs, the optical fundamental mode field and acoustic mode fields are both confined in the core and the inner cladding of TAFs, as shown in Fig. 19. Therefore, no matter how the refractive index distribution of the trench is changed, it will not have any effect on the optical and acoustic mode fields, and TAF's BGS will not change.

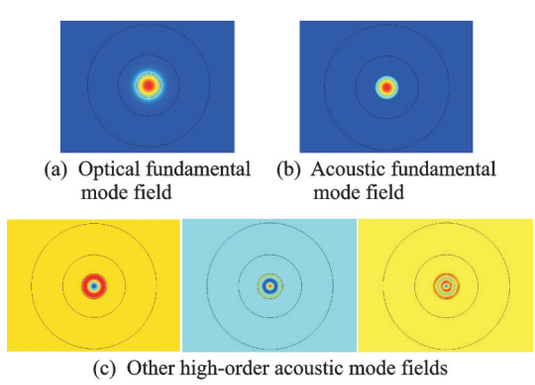

Fig. 19 Calculation results of TAF model by FEA method

Therefore, under the condition that the core radius and refractive index remain unchanged, the TAFs has the only one BGS. Fig.20 shows the total BGS of TAFs and the contribution of each acoustic mode to the total BGS.

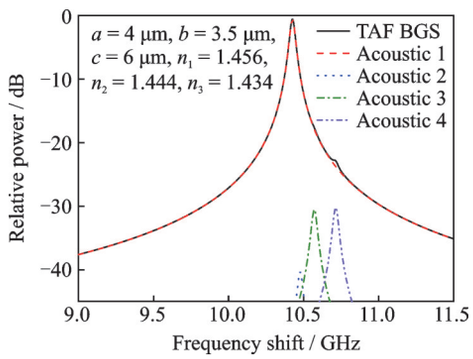

Fig.20 BGS of TAF

In general, changing the position, depth and width of the TAF's trench has no effect on its BGS. TAF used in this section has four acoustic modes, but only a strong main peak and a small secondary peak are reflected on BGS. Therefore, TAF is not suitable for Brillouin fiber sensing, but more suitable for fiber communication, which is also the original intention of its design.

2.5 Comparison of three types of fibers

In the case of two simpler structures, SIOF and GIOF, we have found that the change in total Brillouin gain and acoustic mode number due to the change of core radius and refractive index difference. Briefly, there are up to four acoustic modes in SIOFs and up to six acoustic modes exist in GIOFs. Both of them tend to have high Brillouin gain where the core refractive index is high. The Brillouin gain distributions of SIOFs and GIOFs are roughly consistent with their respective acoustic mode number distributions. For CIOFs, LEAF and TAF are chosen as the typical optical fibers. In LEAFs simulation, we found that due to the existence of the outer-ring section, it usually guides more than five acoustic modes. In addition, LEAF-type optical fibers with a larger g_{B_total} are in the range of n_1 from 1.472 to 1.475, n_2 from 1.444 to 1.46, and c from 10 μm to 15 μm. In regard to the TAFs, the existence of the trench has no effect on their BGSs. In summary, for optical fiber communication, one should choose CIOFs as the working fiber, and the corresponding parameter combination is described in Section 2.4. The SIOFs with core radius from 1.5 μm to 2 μm and core refractive index from 1.465 to 1.474 2 are better for Brillouin sensing application.

3 An Example: Choosing a Fiber Used for Temperature Sensing Based on BBS Power Detection

In our previous work, distributed temperature measurement method based on Brillouin beat spectrum was proposed[12]. Compared with other Brillouin sensing systems that have the shortcomings such as time-consuming, expensive, and complicated, BBS has its advantage of fast, simple and convenient. This method detects the peak power of the Brillouin beat spectrum and uses the homodyne BOTDR system to achieve temperature measurement. From the previous content of this work, we know that multiple acoustic modes can exist in some fibers, corresponding to the different peaks of their BGSs. And the BBS corresponds to the beats between the main peak and the other peaks in BGSs.

The power of Brillouin scattering light in BOTDR is[37]

$$P_B(z)=P_P(0)\exp(-2\alpha z)\alpha_B S\frac{c'W}{2n_{eff}} \quad (20)$$

where $P_P(0)$ is the incident light power, α=0.2 dB/km the fiber's attenuation coefficient at the wavelength of 1.55 μm, c' the velocity of light in vacuum, W the incident pulse width, α_B the Brillouin scattering-loss coefficient[38] and S the backscatter capture fraction[39]. Now we substitute the Brillouin frequency shift $\nu_m=2n_{eff}V_l/\lambda$ into Eq.(4) and rewrite Eq.(20) as an expression with the Brillouin peak gain g_m

$$P_{Bm}(z)=P_P(0)\exp(-2\alpha z)\frac{A}{n_{eff}^2A_{eff}}\cdot g_m \quad (21)$$

where $A=c'^2\pi\omega KTW/6V_l$, ω is the FWHM of the corresponding peak in BGS, K the Boltzmann's constant, and T the absolute temperature. Longitudinal mode acoustic velocity V_l can be expressed as[40]

$$V_l=\sqrt{\frac{E(1-k)}{(1+k)(1-2k)\rho}} \tag{22}$$

The peaks of BBS vary when the peak powers of different BGS peaks change caused by variation of temperature. The dependences of the BBS peak power ΔP_B on temperature can be expressed as[12]

$$\Delta P_B(T)/P=C_{PT}\Delta T \tag{23}$$

where C_{PT} is the temperature coefficient of the BBS peak power and the ΔT the change in temperature.

In the BBS of the fibers with several acoustic modes, the beat peak (i, j) is corresponding to the peak i and peak j in the BGS. If the peak power of the peak i and peak j are respectively P_{Bi} and P_{Bj}, the peak power of the beat peak (i, j) in the BBS is

$$P=2\sqrt{P_{Bi}P_{Bj}} \tag{24}$$

If the power measurement uncertainty of the detection system is ΔP, then the measurement uncertainty of BBS peak power in the form of relative percentage value δP will be

$$\delta P=\frac{\Delta P}{2\sqrt{P_{Bi}P_{Bj}}} \tag{25}$$

and the temperature measurement uncertainty is

$$\delta T=\delta P/C_{PT} \tag{26}$$

In Eq.(25), the power measurement uncertainty ΔP originates from the detection or measurement error of the detectors and photoelectric instruments of the BBS system. When the BBS power detection works with a certain fiber as the sensor, then the smaller the value of δP, the higher the accuracy of temperature measurement. It can be seen from the above equations that the measurement accuracy depends on the relative peak intensity of the multi-peak BGS. Therefore, in order to enable the BBS system to have higher measurement accuracy, fibers with high Brillouin gain and(or) similar peak gain in their multimodal BGSs are needed.

Now, we name the fiber with the 1st BGS in Fig. 5 as SIOF-1, the fiber with the 1st BGS in Fig. 8 as GIOF-1, the fiber with the 1st BGS in Fig.13 as LEAF-1, and the fiber with BGS in Fig.20 as TAF, and so on. SIOF-3, SIOF-4, GIOF-5, GIOF-6, LEAF-5 to LEAF-9 and TAF are selected as the research objects to discuss the influence of total Brillouin gain and similar peak gain on the BBS measurement accuracy.

We continue to use the above setting for relative power, set the main peak power of the SIOF-4's BGS to 0 dBm, and the the temperature coefficient of all fibers to 29.5×10^{-4} °C[12]. The power measurement uncertainty ΔP of the BBS detection system set to 0.1% of the maximum detection power. The simulation results are shown in Table 5.

Table 5 Temperature measurement accuracy of different fibers

Fiber	P_{B1}/ dBm	P_{B2}/ dBm	$\sqrt{P_{B1}P_{B2}}$/ dBm	δP/ 10^{-3}	δT/ ℃
SIOF-4	0.00	−23.08	−11.54	7.13	2.42
SIOF-3	−1.09	−14.77	−7.93	3.10	1.05
GIOF-5	−1.33	−8.46	−4.90	1.54	0.52
GIOF-6	−1.08	−8.39	−4.73	1.49	0.50
LEAF-5	−2.64	−5.00	−3.82	1.20	0.41
LEAF-6	−2.55	−4.95	−3.75	1.19	0.40
LEAF-7	−4.18	−5.76	−4.97	1.57	0.53
LEAF-8	−2.89	−5.13	−4.01	1.26	0.43
LEAF-9	−1.74	−6.28	−4.01	1.26	0.43
TAF	−0.56	−22.85	−11.70	7.40	2.51

From the Table 4, we can see that even though the SIOF-4 has the largest Brillouin main peak gain g_1 and the maximum detection power P_{B1}, the peak gain of its secondary peak is very low, making the corresponding detection power small, so the peak power of the beat peak(1, 2) is small and its temperature measurement uncertainty is relatively poor. Meanwhile, LEAF-6 has a small peak intensity difference, so the beat power of peak 1 and peak 2 in its BGS is larger, and it shows the best temperature measurement accuracy.

Based on a comprehensive analysis of the simu-

lation results of the above three types of fibers, the LEAF-type fiber represented by the 6th spectrum in Fig.13 has a large total Brillouin gain and the intensity of the three peaks in the BGS is the closest. Its second and third peaks are 2.4 and 8.1 dB weaker than the main peak, respectively. In such a fiber, the inner-core radius, inner-cladding radius, and outer-core radius are 3.04, 4, 8 μm, respectively. Furthermore, the fiber axis refractive index, outer-core refractive index, and cladding refractive index are 1.475, 1.452, and 1.444, respectively.

The relative power of first three main peaks of the LEAF's BGS in Ref.[12] are 0, −16.5 and −19 dB when utilized in BBS optical fiber sensing system. Assuming that the sum of the three peaks' power of the Corning's LEAF is equal to that of the proposed new fiber (denoted as P_A), then three peak powers of Corning's LEAF are $0.97P_A$, $0.02P_A$ and $0.01P_A$, respectively. Similarly, the relative power of first three main peaks of the proposed fiber are 0, −2.4 and −8.1 dB and their peak powers can be expressed as $0.58P_A$, $0.33P_A$ and $0.09P_A$. According to Eq.(23), the ratio of Corning's LEAF's and new fiber's power measurement uncertainty of the detection system δP can be expressed as

$$\frac{\delta P_{(1,2)}}{\delta P'_{(1,2)}} = \frac{P_A\sqrt{0.58\times 0.33}}{P_A\sqrt{0.97\times 0.02}} = 3.1 \qquad (27)$$

We once again assume that the Corning's LEAF and the fiber we designed have the same power-temperature in sensing system, that is, compared with the original fiber, the SNR of the new fiber's beat peak(1,2) is 3.1 times higher when used in BBS sensing system. It could be the most suitable fiber used in the optical fiber sensing system based on BBS.

4 Conclusions

The new and full images of Brillouin gain and acoustic modes number of the fiber as a function of the refractive index distribution are presented by using FEA method. When using the FEA method to solve the acoustic field in the fiber, a new method is also proposed that can be used to quickly obtain the circular symmetric acoustic mode solution, which greatly improves the simulation efficiency. The influence of refractive index distribution on the BGS in commonly used GeO_2-doped optical fibers, including step-index, graded-index, and complex-index optical fibers, are discussed by considering the influence of changing the refractive index difference and the geometric size simultaneously. The refractive index distribution in fibers determines the total Brillouin gain, acoustic mode number, and peak intensity difference of the BGS. From the results of the SIOFs, we can conclude that fibers with more acoustic modes also exhibit higher Brillouin gain. And when the core radius is from 1.5 μm to 2 μm, and the refractive index difference is as large as possible, the total Brillouin gain is greater than that in other cases. For the GIOFs, the distribution of the total Brillouin gain is similar to that of SIOFs. And when the core radius is from 2 μm to 3 μm, and the refractive index difference is as large as possible, the total Brillouin gain is greater. Both of them tend to have high Brillouin gain where the core refractive index is high. And the Brillouin gain distributions of the SIOFs and the GIOFs are roughly consistent with their respective acoustic mode number distributions. As for LEAF-type complex index fibers, the number of acoustic modes is generally greater than or equal to five due to the presence of an outer-ring section. And the relative power difference between the adjacent peaks is small in LEAFs. For trench assisted fiber, the existence of trench has no effect on its BGS. We also obtain a special CIOF with a RIP in LEAF model as a sensing fiber used in sensing system based on BBS, and its fiber axis refractive index, outer-ring refractive index, cladding refractive index are 1.475, 1.452, 1.444, and its inner-core radius, inner-cladding radius, and outer-core radius are 3.04, 4, and 8 μm, respectively. Compared with the original LEAF fiber, the SNR of the

new fiber's beat peak (1, 2) is 3.1 times higher when used in BBS sensing system.

References

[1] AGRAWAL G P. Nonlinear fiber optics[M]. 5th ed. New York: Academic Press, 2013.

[2] KOBYAKOV A, KUMAR S, CHOWDHURY D Q, et al. Design concept for optical fibers with enhanced SBS threshold[J]. Optics Express, 2005, 13(14): 5338-5346.

[3] LI M J, CHEN X, WANG J, et al. Al/Ge co-doped large mode area fiber with high SBS threshold[J]. Optics Express, 2007, 15(13): 8290-8299.

[4] XUAN L, BAO X. Brillouin spectrum in LEAF and simultaneous temperature and strain measurement[J]. Journal of Lightwave Technology, 2012, 30(8): 1053-1059.

[5] ZOU W, HE Z, HOTATE K. Acoustic modal analysis and control in W-shaped triple-layer optical fibers with highly-germanium-doped core and F-doped inner cladding[J]. Optics Express, 2008, 16(14): 10006-10017.

[6] SHIBATA N, AZUMA Y, HORIGUCHI T, et al. Identification of longitudinal acoustic modes guided in the core region of a single-mode optical fiber by Brillouin gain spectra measurements[J]. Optics Letters, 1988, 13(7): 595.

[7] SHIBATA N, OKAMOTO K, AZUMA Y, et al. Longitudinal acoustic modes and Brillouin-gain spectra for GeO_2-doped-core single-mode fibers[J]. Journal of the Optical Society of America B, 1989, 6(6): 1167-1174.

[8] SABATIER C, GIRARD S, MESCIA L, et al. Combined experimental and simulation study of the fiber composition effects on its Brillouin scattering signature[J]. Journal of Lightwave Technology, 2019, 37: 4619-4624.

[9] JEN C K, NERON C, SHANG A, et al. Acoustic characterization of silica glasses[J]. Journal of the American Ceramic Society, 2010, 76(3): 712-716.

[10] KOYAMADA Y, SATO S, NAKAMURA S, et al. Simulating and designing brillouin gain spectrum in single-mode fibers[J]. Journal of Lightwave Technology, 2004, 22(2): 631-639.

[11] MI L, JIAO W, LIU W X, et al. A method for peak-seeking of BOTDR based on the incomplete Brillouin spectrum[J]. IEEE Photonics Journal, 2015, 7(5): 1-10.

[12] LU Y, QIN Z, LU P, et al. Distributed strain and temperature measurement by Brillouin beat spectrum[J]. IEEE Photonics Technology Letters, 2013, 25(11): 1050-1053.

[13] DIAKARIDIA S, YUE P, XU P, et al. Detecting cm-scale hot spot over 24-km-long single-mode fiber by using differential pulse pair BOTDA based on double-peak spectrum[J]. Optics Express, 2017, 25(15): 17727-17736.

[14] CUI Q, PAMUKCU S, WEN X, et al. Distributed fiber sensor based on modulated pulse base reflection and Brillouin gain spectrum analysis[J]. Applied Optics, 2009, 48(30): 5823.

[15] DONG Y, ZHANG H, CHEN L, et al. 2 cm spatial-resolution and 2 km range Brillouin optical fiber sensor using a transient differential pulse pair[J]. Applied Optics, 2012, 51(9): 1229-1235.

[16] GU Haidong, DONG Huijuan, ZHANG Guangyu, et al. Simultaneous measurement of pressure and temperature using dual-path distributed Brillouin sensor[J]. Applied Optics, 2015, 54(11): 3231-3235.

[17] SHIRAKI K, OHASHI M, TATEDA M. SBS threshold of a fiber with a Brillouin frequency shift distribution[J]. Journal of Lightwave Technology, 1996, 14(1): 50-57.

[18] NIKLES M, THEVENAZ L. Brillouin gain spectrum characterization in single-mode optical fibers[J]. Journal of Lightwave Technology, 1997, 15(10): 1842-1851.

[19] XING C, KE C J, GUO Z, et al. Distributed multi-parameter sensing utilizing Brillouin frequency shifts contributed by multiple acoustic modes in SSMF[J]. Optics Express, 2018, 26(22): 28793-28807.

[20] ABEDIN K S. Observation of strong stimulated Brillouin scattering in single-mode As2Se3 chalcogenide fiber[J]. Optics Express, 2005, 13(25): 10266-10271.

[21] ABEDIN K S. Stimulated Brillouin scattering in single-mode tellurite glass fiber[J]. Optics Express, 2006, 14(24): 11766-11772.

[22] DRAGIC P D, KUCERA C, BALLATO J, et al. Brillouin scattering properties of lanthano-aluminosilicate optical fiber[J]. Applied Optics, 2014, 53(25): 5660-5671.

[23] RUFFIN A B, LI M J, CHEN X, et al. Brillouin

gain analysis for fibers with different refractive indices[J]. Optics Letters, 2005, 30(23):3123-3128.

[24] MIZUNO Y, ISHIGURE T, NAKAMURA K. Brillouin gain spectrum characterization in perfluorinated graded-index polymer optical fiber with 62.5-μm core diameter[J]. IEEE Photonics Technology Letters, 2011, 23(24):1863-1865.

[25] DASGUPTA S, POLETTI F, SHENG L, et al. Modeling Brillouin gain spectrum of solid and microstructured optical fibers using a finite element method[J]. Journal of Lightwave Technology, 2010, 29(1):22-30.

[26] KOBYAKOV A, SAUER M, CHOWDHURY D. Stimulated Brillouin scattering in optical fibers[J]. Advances in Optics and Photonics, 2009, 2(1):1-59.

[27] CHERIF R, ZGHAL M, TARTARA L. Characterization of stimulated Brillouin scattering in small core microstructured chalcogenide fiber[J]. Optics Communications, 2012, 285(3):341-346.

[28] CHENG T, CHERIF R, LIAO M, et al. Stimulated Brillouin scattering of higher-order acoustic modes in four-core tellurite microstructured optical fiber[J]. Applied Physics Express, 2012, 5(10):2501.

[29] SAKAMOTO T, YAMAMOTO T, SHIRAKI K, et al. Low distortion slow light in flat Brillouin gain spectrum by using optical frequency comb[J]. Optics Express, 2008, 16(11):8026-32.

[30] CHAO J, LIANG W, CHEN Y, et al. Single-measurement digital optical frequency comb based phase-detection Brillouin optical time domain analyzer[J]. Optics Express, 2017, 25(8):9213.

[31] QIAN, WANG, GERALD, et al. Theoretical and experimental investigations of macro-bend losses for standard single mode fibers[J]. Optics Express, 2005, 13(12):4476-4484.

[32] GARRETT I, TODD C J. Components and systems for long-wavelength monomode fibre transmission[J]. Optical & Quantum Electronics, 1982, 14(2): 95-143.

[33] AOKI Y, TAJIMA K, MITO I. Input power limits of single-mode optical fibers due to stimulated Brillouin scattering in optical communication systems[J]. Journal of Lightwave Technology, 1988, 6(5): 710-719.

[34] CHI R, LI L, LI X, et al. Stimulated Brillouin scattering suppressed EDFA in a long-haul optical fiber link system[C]// Proceedings of International Conference on Optical Communications & Networks. [S.l.]: IEEE, 2015.

[35] GAMBLING W A, PAYNE D N, MATSUMURA H. Cut-off frequency in radially inhomogeneous single-mode fibre[J]. Electronics Letters, 1977, 13(5): 139-140.

[36] MALITSON I H. Interspecimen comparison of the refractive index of fused silica[J]. Journal of the Optical Society of America, 1965, 55:1205-1208.

[37] HORIGUCHI T, TATEDA M. BOTDA-nondestructive measurement of single-mode optical fiber attenuation characteristics using Brillouin interaction: Theory[J]. Journal of Lightwave Technology, 1989, 7(8):1170-1176.

[38] RICH T C, PINNOW D A. Evaluation of fiber optical waveguides using Brillouin spectroscopy[J]. Applied Optics, 1974, 13(6):1376-1378.

[39] AOYAMA K, NAKAGAWA K, ITOH T. Optical time domain reflectometry in a single-mode fiber[J]. IEEE Journal of Quantum Electronics, 1981, 17(6): 862-868.

[40] TIMOSHENKO S P, GOODIERWRITED J N. Theory of elasticity[M].3rd ed. New York: McGraw-Hill Book Company, 1970.

Acknowledgements This work was supported by the National Natural Science Foundation of China (Nos.61875086, 61377086), the Aerospace Science Foundation of China (No.2016ZD52042) and the Foundation of Graduate Innovation Center in Nanjing University of Aeronautics and Astronautics (No. kfjj20170801).

Authors Mr. **JI Zhengyuan** received his B.S. degree from Nantong University, Nantong, China, in 2018. He is working toward the Ph.D. degree in optical engineering at the Nanjing University of Aeronautics and Astronautics, Nanjing, China. His research focuses on Brillouin sensing and Brillouin fiber laser.

Prof. **LU Yuangang** is currently a full professor of the College of Science, Nanjing University of Aeronautics and Astronautics, Nanjing, China. His research interests include optical metrology, optical information processing, and optical fiber sensing.

Author contributions Mr. **JI Zhengyuan** contributed to calculation and simulation and writing the manuscript. Prof. **LU Yuangang** designed and guided the study, and gave key

opinions on the core issues. Mr. **PAN Yuhang** designed the simulation and wrote the first draft. Mr. **PENG Jianqin** and Mr. **ZHANG Zelin** condected some related work about the simulation. Prof. **WANG Jiming** contributed to the background of the study. All authors commented on the manuscript draft and approved the submission.

Competing interests The author declare no competing interests.

(Production Editor: SUN Jing)

二氧化锗掺杂光纤中折射率分布对布里渊增益谱的影响

吉正源[1,2]，路元刚[1,2]，潘宇航[2,3]，彭楗钦[1,2]，张泽霖[1,2]，王吉明[2]

(1.南京航空航天大学航天学院空间光电探测与感知工业和信息化部重点实验室，南京 211106，中国；
2.南京航空航天大学理学院，南京 211106，中国；3.上海飞机设计研究院，上海 200120，中国)

摘要：二氧化锗通常用作掺杂剂来调控光纤中的折射率分布(Refractive index profile，RIP)和声速分布(Acoustic velocity profile，AVP)，从而在光纤中形成不同的布里渊增益谱(Brillouin gain spectrum，BGS)特性，如布里渊增益、声模式数和峰强度差。当光纤用于光纤传感或光纤通信系统时，其BGS特性可能在确定系统性能方面起重要作用。本文通过有限元分析法(Finite element analysis，FEA)研究阶跃折射率光纤、渐变光纤以及复杂折射率分布光纤中RIP及相应的AVP对布里渊增益谱的影响。提出了一种新的方法，可以有效分辨出声模式解，同时改变光纤折射率分布与几何尺寸，获得光纤总布里渊增益和声模式数同折射率分布关系的新的完整图像。对于每一类光纤，提供了用于光纤传感与光纤通信的建议参数。探索并找到了具有相近布里渊峰强度的多峰布里渊增益谱的光纤，该光纤能够用于布里渊拍频谱检测并提高传感精度。

关键词：布里渊增益谱；光纤；声学模式；折射率；有限元分析